

Classifying self-gravitating radiations

Hyeong-Chan Kim^{1,2,*}

¹*Department of Physics, North Carolina State University, Raleigh, NC 27695-8202, USA*

²*School of Liberal Arts and Sciences, Korea National University of Transportation, Chungju 380-702, Korea*

We study a static system of self-gravitating radiations confined in a sphere by using numerical and analytic calculations. We classify and analyze the solutions systematically. Due to the scaling symmetry, most of main properties of a solution can be represented as a segment of a solution curve on a plane of two-dimensional scale invariant variables. We define a *fake horizon* from the analogy to an apparent horizon. A given solution is uniquely characterized by three parameters representing the solution curve, the size of the fake horizon, and the sphere size. Given the data, a fake horizon exists if the sphere size is larger than that of the fake horizon. We additionally present an analytic solution on the verge of forming a blackhole.

PACS numbers: 04.40.Nr, 04.40.-b, 04.20.Jb

Keywords: self-gravitating radiation, exact solution, horizon

I. INTRODUCTION

A bounded self-gravitating isothermal sphere are an interesting object as a model of a small dense nucleus of stellar systems, which is to some extent independent of the outer parts of the system [1]. In 1981, a spherically symmetric solution of self-gravitating radiation was presented by Sorkin, Wald, and Jiu [2] as a solution that maximizing the entropy based on general relativity. The heat capacity and stability of the solution were further analyzed in Refs. [3] and [4–6]. Schmidt and Homann [7] named the geometry ‘photon star’. Thereafter, the system has drawn attentions repeatedly in relation to the entropy bound [8, 9], maximum entropy principle [10–12], holographic principle [13–15], blackhole thermodynamics [16], and exclusion of blackhole firewalls [17]. Self-gravitating radiation in Anti-de Sitter spacetime was also pursued [18–20]. Studies on the systems of self-gravitating perfect fluids are undergone [21]. An interesting extension of the self-gravitating system was presented in Ref. [7, 22] where a conical singularity was included at the center as an independent source from the radiation. The singularity was said to be benign in the sense that it does not give rise to inextensible causal geodesics. Because no timelike geodesics reach the singularity and null geodesics simply pass it. A thermodynamic interpretation for the conical singularity was also discussed [22]. Analytic analysis was presented for an extreme case, which was interpreted as a spacetime blackhole with perfect fluid in equilibrium [23]. Some of the singular solutions were shown to have an interesting geometry, which resembles an event horizon to an outside observer. The solutions can also be used to study a spherical shell of self-gravitating radiations once one places an inner boundary after excising the central part. However, we notice that the understanding on the details of the geometry is not satisfactory because its geometric structure is not classified and analyzed throughly. The purpose of the present work is to make up for this part. The key idea of this work is to characterize the spherically symmetric systems by means of parameters related to their specific properties. We also generalize the analytic analysis done by Zurek and Page [23].

Let the sphere of radiations has a radius R . Outside the sphere, the spacetime is described by the vacuum Schwarzschild metric with Arnowitt-Deser-Misner (ADM) mass M_R . The system is different from an ordinary star whose boundary is implemented by its own gravity and equation of state. In the absence of an artificial boundary at R , the density of the static solution becomes proportional to $1/r^2$ as $r \rightarrow \infty$. Then, the energy of the system goes to infinity and stability issues also arise. Despite with this difference, we call it a ‘star’ later in this work for convenience. The metric inside was shown [22] to be given by

$$ds^2 = - \left(1 - \frac{2M_R}{R} \right) \sqrt{\frac{\rho(R)}{\rho(r)}} dt^2 + \frac{dr^2}{1 - 2m(r)/r} + r^2(d\theta^2 + \sin^2\theta d\phi^2), \quad r \leq R, \quad (1)$$

where $m(r)$ and $\rho(r)$ are the mass inside and the density at r , respectively. The energy density is related with the

*Electronic address: hckim@ut.ac.kr

mass as

$$\rho(r) = \frac{1}{4\pi r^2} \frac{dm(r)}{dr}. \quad (2)$$

Because the system is composed of radiations, it also satisfies $\rho(r) = 3p(r)$, where $p(r)$ denotes the pressure at r . From the blackbody radiation law, the surface energy density is given by $\rho(R) = \sigma T^4$, where T denotes the locally measured temperature at R and σ is the Stefan-Boltzmann constant.

The structure of the system is described by the Tollman-Oppenheimer-Volkoff (TOV) equation for the metric (1). Introducing a dimensionless variable

$$u \equiv \frac{2m(r)}{r}, \quad (3)$$

The TOV equation can be cast into a second order differential equation for u as

$$\frac{1}{6}(u + u')(u + u' + 3) + (u - 1)\left(u + u' - \frac{u' + u''}{4}\right) = 0, \quad (4)$$

where prime denote the derivative with respect to a dimensionless variable

$$\xi = \log \frac{r}{r_H}, \quad (5)$$

and r_H is a length scale which will be specified later. The equation (4) does not contain any length scale. Therefore, the system possesses a scaling symmetry: The transformation $(m \rightarrow e^s m, r \rightarrow e^s r)$ preserves the equation of motions. As a result, various properties of the solutions can be described by scale invariant variables. Introducing a scale-invariant variable v ,

$$v \equiv \frac{dm(r)}{dr} = 4\pi r^2 \rho(r) = \frac{u + u'}{2}, \quad (6)$$

the TOV equation (4) can be rewritten as a first order differential equation for u and v ,

$$\frac{dv}{du} = f(u, v) \equiv \frac{2v(1 - 2u - 2v/3)}{(1 - u)(2v - u)}. \quad (7)$$

The integral curve of Eq. (7) on the plane (u, v) is called a solution curve which is denoted by C in this work. The allowed range of (u, v) is $u < 1$ and $v \geq 0$, where each inequality represents the fact that the spacetimes is static and the energy density of radiation is non-negative, respectively. Note that any solution curve becomes parallel to the u axis when it crosses the line

$$P : 2u + 2v/3 = 1 \quad (8)$$

and parallel to the v axis when it crosses the line

$$H : u = 2v. \quad (9)$$

This property indicates that a solution curve will spiral around the point $(u, v) = (3/7, 3/14)$, which point is an end of every solution curves. The solution curves are divided into two classes by means of the other end, which corresponds to the center of the star. One class is composed of a solution curve which begins at $(u, v) = (0, 0)$. The solution curve, namely C , describing solutions of pure radiation were found in Ref. [2] as a stable static configuration, where the word ‘pure’ implies that the system does not contain mass contributions other than the radiation. The other class of solution curves describe spacetimes bearing a negative mass source at the center which presents a conical singularity. The curves originate from $(u, v) \rightarrow (-\infty, 0)$.

In this work, we aim two separate purposes. First is to classify and parametrize the solutions of self-gravitating radiations systematically so that the properties of the solution is visible. For this purpose, we classify the solution curves and analyze the properties of the solutions in Sec. II and Sec. III. The solutions bearing a conical singularity at the center were known [22] that they can be divided into two separate classes, those with and without a wall (deformed horizon-like object). However, a clear criteria for the classification and a clear definition for the horizon-like object is absent, which we are seeking in this work. Second is to extend analytic solutions for extreme cases. Because of the geometric similarity between a *fake horizon* and an apparent horizon, we hope to describe its geometry analytically. In Sec. IV, we provide an analytic solution describing the state when the *fake horizon* is close to an apparent horizon. We summarize and discuss the results in Sec. V.

II. PROPERTIES FOR SELF-GRAVITATING RADIATION

A. Scale transformation

Let us parametrize a solution curve C_ν of Eq. (7) in terms of ξ as $(u(\xi), v(\xi))$, where ν is a parameter characterizing the curve which will be specified later. The parametrization is determined by Eq. (6) which determines the radius as $r(\xi)$. Note that, from Eq. (5), the values of u and v at each point on the curve are invariant under the scaling,

$$m \rightarrow \bar{m} = e^s m, \quad r \rightarrow \bar{r} = e^s r, \quad \xi \rightarrow \bar{\xi} = \xi + s, \quad u(\xi) \rightarrow \bar{u}(\bar{\xi}) = u(\xi), \quad v(\xi) \rightarrow \bar{v}(\bar{\xi}) = v(\xi). \quad (10)$$

Therefore, $\bar{u}(\xi) = u(\xi - s)$ represents a new solution of Eq. (4) with its mass and radius are scaled. Explicitly, the surface values (u_R, v_R) are invariant,

$$\bar{u}(\xi_R + s) = u(\xi_R) = \frac{2M_R}{R}, \quad \bar{v}(\xi_R + s) = v(\xi_R) = 4\pi R^2 \rho(R), \quad (11)$$

where $M_R = m(R)$. On the other hand, the mass, the radius, and the density scale as

$$\bar{m}(e^s R) = e^s M_R, \quad \bar{R} = e^s R, \quad \bar{\rho}(e^s R) = e^{-2s} \rho(R). \quad (12)$$

In addition, the range of ξ is changed from $(-\infty, \xi_R]$ to $(-\infty, \xi_R + s]$. Given a solution $u(\xi)$ supported with the boundary value at $r = R$, the scale transformation provides a set of solutions having scaled mass and density related by Eq. (12). In fact, any point on C_ν can play the role of a boundary point which supports a set of solutions related by the scale transform. In this sense, a solution curve C_ν provides a set of solutions parameterized by R and s .

B. The central region

Let us study the behaviors of the solutions to Eq. (4) around the origin with $\xi \ll -1$. Eq. (4) allows two different small r behaviors,

$$m_r(r) = \frac{\kappa r_H}{6} \left(\frac{r}{r_H} \right)^3, \quad m_s(r) = \frac{r_H}{2} \left[-\mu_0 + \frac{\kappa}{5} \left(\frac{r}{r_H} \right)^5 \right]. \quad (13)$$

We scale the mass and radius in terms of r_H to encompass the scale symmetry. The first one, $m_r(r)$, corresponds to the regular solution which will be discussed in subSec. III A. The second one, m_s , must be negative at the origin, implying $\mu_0 > 0$. Because the radiation has positive energy density, κ is required to be positive. The energy density of radiation at the center is $\rho_s = (\kappa/8\pi r_H^2) \times (r/r_H)^2$. Comparing the functional forms of ρ_s with ρ_r , it is evident that the radiation is repelled from the center by the negative mass at the central singularity.

We next consider how the solutions (13) change with respect to the scaling. Through the scale transformation (10), the coefficients κ and μ_0 should change. Let us consider the case of regular solution, $m_r(r)$, first. Under the scaling in Eq. (10), the functional form of m_r in Eq. (13) changes to

$$\bar{m}_r(\bar{r}) = e^s m_r(r) \quad \Rightarrow \quad \bar{m}_r(\bar{r}) = \frac{\kappa \bar{r}_H}{6} \left(\frac{\bar{r}}{\bar{r}_H} \right)^3, \quad (14)$$

where we use the transformation law of the referential point (12) and $\bar{r}_H = e^s r_H$ is the transformed radius of r_H . Omitting bar in \bar{r} in Eq. (14), the functional form of the scaled solution is the same as the original one with the replacement $\kappa \rightarrow \kappa e^{-2s}$. Therefore, once one finds a solution for given κ , the central form of all other solutions related by the scaling is also at hand.

For the case of the solution $m_s(r)$, the scaling (10) leads to

$$\bar{m}_s(\bar{r}) = \frac{\bar{r}_H}{2} \left[-\mu_0 + \frac{\kappa}{5} \left(\frac{\bar{r}}{\bar{r}_H} \right)^5 \right]. \quad (15)$$

Note that the functional form of the scaled solution is, omitting bar in \bar{r} , the same as the original one with the replacements $\mu_0 \rightarrow e^s \mu_0$ and $\kappa \rightarrow e^{-4s} \kappa$. With this form, the explicit functional dependence on the scale becomes evident. Note that the mass, $-\bar{r}_H \mu_0$, of the conical singularity changes with the scale.

C. Asymptotic behaviors

We next consider the asymptotic behavior as $\xi \rightarrow \infty$. By assuming solutions in the form, $u = ae^{-\xi} + b$, one may find that the differential equation (4) allows two different asymptotic forms for $u(\xi)$,

$$u_a \rightarrow \frac{3}{7}, \quad u_t \rightarrow ae^{-\xi}, \quad (16)$$

where a is an arbitrary constant. With the increase of ξ , u_a acts as if it is an attractor which pulls every nearby solutions (Here, we interpret as if ξ is a time even though it is a radial coordinate). Introducing a small perturbation, the solution of Eq. (4) with first nonvanishing contribution takes the form,

$$u_a = \frac{3}{7} \left[1 + \tilde{c}_1 e^{-3\xi/4} \cos \left(\frac{\sqrt{47}}{4} \xi + \tilde{\phi} \right) \right] \Rightarrow m_a(r) = \frac{3r}{14} \left[1 + \tilde{c}_1 \left(\frac{r_H}{r} \right)^{3/4} \cos \left(\frac{\sqrt{47}}{4} \log \frac{r}{r_H} + \tilde{\phi} \right) \right], \quad (17)$$

where \tilde{c}_1 and $\tilde{\phi}$ are integration constants. On the (u, v) plane, the curves satisfies

$$\left(u - \frac{3}{7} \right)^2 + \frac{64}{47} \left(v - \frac{3}{8}u - \frac{3}{56} \right)^2 = \left(\frac{3\tilde{c}_1}{7} \right)^2 \left(\frac{r}{r_H} \right)^{-3/2}. \quad (18)$$

The solution curves spire in to the point $(u, v) = (3/7, 3/14)$ as r increases. For the asymptotic form (17), the scale transform (10) is achieved by $r_H \rightarrow \bar{r}_H$.

The other asymptotic form, $u_t(\xi)$, approaches zero and $v_t(\xi) = 0$ for all ξ . The asymptotic form plays the role of an attractor when the radius r (equivalently ξ) decreases from infinity. Small perturbations around u_t

$$u = u_t + \delta(\xi) = ae^{-\xi} + \epsilon e^{2\xi} \Rightarrow m_t(r) = \frac{a}{2} + \frac{\epsilon}{2} \left(\frac{r}{r_H} \right)^3, \quad (19)$$

increase indefinitely as $r \rightarrow \infty$ to make the solution leave u_t permanently, where ϵ is a tiny integration constant. However, as will be shown later, in the presence of a strong *fake horizon*, this almost constant mass region becomes wide enough to regard Eq. (19) as an approximate asymptotic form for $r \gg r_H$.

Eq. (16) may not be realized unless the outer boundary is located in the asymptotic region. For most cases, noting the heat capacity in Ref. [3]¹, an instability appears at a smaller radius than r_H making the system be unstable. However, as noted in Ref. [22], the conical singularity may play some role in thermodynamics and affect to the stability. In this sense, the issue of stability needs additional research. To avoid the complexity due to the conical singularity, an inner boundary will be required which prohibits the radiation from incoming.

D. Fake horizon

Most solutions other than the regular one have a conical singularity at the center [22]. Based on Newtonian gravity, objects having positive masses attract each other. Similarly, the radiations are attracted to the center due to their self-gravity. On the other hand, the negative mass at the center repels the radiations. The balance of the two behaviors concentrates the density at some intermediate region. Therefore, in the presence of large negative mass at the center and a large quantity of radiations outside enough to compensate the repulsion, a region of strong gravity will be developed. To represent this phenomena, we define a *fake horizon*.

Consider a metric of the form,

$$ds^2 = h_{ab}(x^c) dx^a dx^b + r^2 d\Omega_{(2)},$$

where $a, b, c = 0, 1$ and $r(x^a)$ is a scalar function of x^0 and x^1 . An apparent horizon for the metric is defined by the surface satisfying

$$\chi^2 \equiv h^{ab} \nabla_a r \nabla_b r = 0. \quad (20)$$

¹ The heat capacity was calculated for a regular solution. However, the same formula holds for other solutions up to the contribution of central singularity.

At the apparent horizon, the vector field $\nabla_a r$ becomes null. For the metric ansatz (1), the coordinate change $dr \rightarrow 0$ for a finite proper distance change $\delta r = \sqrt{g_{rr}} dr$. Applying Eq. (20) to the metric (1), the apparent horizon will exist only at the position satisfying $\chi^2 = 1 - 2m(r)/r = 0$. Eq. (7) indicates that this condition is never achieved with the self-gravitating radiation because $du = 0$ at $u = 1$, which implies that a solution curve never cross the line $u = 1$.

If χ^2 is very small at a surface surrounded by thermal radiations, an observer located outside of the region have difficulty in distinguishing the surface from an apparent horizon. Even though photons may propagate over the surface, it would be difficult to discern it from the surroundings. In this sense, we define a *fake horizon* as a surface where χ^2 takes its minimum value for a given solution curve. The local minimization condition of χ^2 for the metric (1) becomes

$$\delta(\chi^2) = 0 \implies u = 2v, \quad \frac{3}{7} < u \leq 1, \quad (21)$$

where the inequality is included because χ^2 is locally maximized on $u = 2v$ for $u < 3/7$. Noting the asymptotic form (18), a solution curve crosses the line H many times. Of all the points, the closest one to $u = 1$ corresponds to the *fake horizon*. In fact, as can be seen in the next section, all the *fake horizon* is located in the region $u_r \leq u < 1$, where $u_r \approx 0.4926$ corresponds to the value of *fake horizon* position of regular solution.

E. Characterizing solution curves

In Refs. [2, 4, 22], the authors identified the solution space in terms of a set of parameters defined at the surface $r = R$. To do this, Eq. (4) was integrated to get the solution curve C inward to $r = 0$ after fixing the boundary value (u_R, v_R) . A lesson from the experiences on the regular solution is that a solution space is conveniently characterized by the combination of a point (u_R, v_R) on the solution curve and the radius R of the system as in Fig. 1. The whole

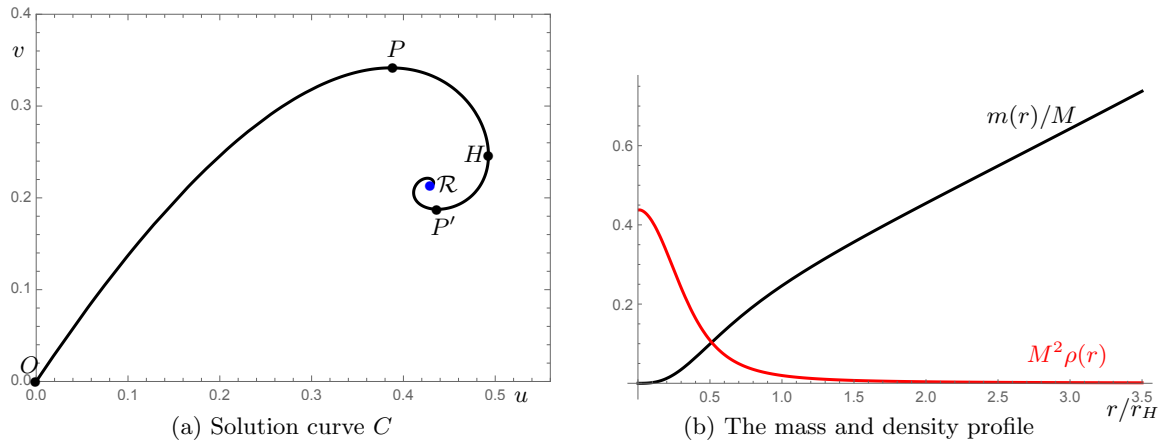


FIG. 1: A regular solution. The solution curve in (a) reproduces Fig. 1 in Ref. [22]. (b) shows typical forms of the mass and density profile. Each point on C corresponds to a boundary data for a regular solution.

solution space can be found once one finds a set of solution curves covering whole physically acceptable region of (u, v) plane. Because the (u, v) plane is two dimensional, the one-dimensional solution curves should be characterized by a parameter, namely, ν . An immediate task is to find out a most convenient parameter for ν . A first impression is to use the central values such as μ_0 or κ in Eq. (13). For example, with the choice of a scaling $e^s = \kappa^{1/4}$, one can choose $\nu \equiv \bar{\mu}_0 = \mu_0 \kappa^{1/4}$ with $\bar{\kappa} = 1$. Even though this choice is relevant theoretically, the solution is too sensitive to a small change of the central values numerically.

At the present work, we choose to characterize the solution curve in terms of

$$\nu \equiv 1 - u_H \quad (22)$$

at the *fake horizon*. With this parametrization, the point H on C_ν is given by

$$H \equiv \left\{ H_\nu \left(1 - \nu, \frac{1 - \nu}{2} \right) \mid 0 < \nu \leq \nu_r \right\}, \quad (23)$$

where the absence of horizon restricts $\nu > 0$ and $\nu_r \approx 0.50735$ corresponds to the regular solution, which value was determined in Ref. [2].

For a given C_ν , the value of u is maximized to be $u_H = 1 - \nu$ at H_ν . By using the scale transform, we may freely choose a referential solution so that $\xi = 0$ at H . Let us consider a system given by the boundary data (R, M_R, T_R) . The boundary values for the scale invariant variables are given by $u_R = 2M_R/R$ and $v_R = 4\pi\sigma R^2 T_R^4$. The solution curve can be parametrized by $\xi = \log(r/r_H)$. Then, the position of the boundary data (u_R, v_R) on the solution curve can be uniquely represented once $\xi_R = \log(R/r_H)$ is known. Therefore, a specific solution is uniquely determined once we know

$$(\nu, r_H, R). \quad (24)$$

Now, the existence of a *fake horizon* is easy to identify. If ξ_R is positive, the star size R is larger than r_H and a *fake horizon* exists. Under the scale transformation, (ν, r_H, R) is mapped to $(\nu, e^s r_H, e^s R)$. ξ_R is invariant because it is defined from the ratio of two radius of the star and of the *fake horizon*, both are co-variant.

III. VARIOUS SOLUTIONS

Any point (u_R, v_R) on the solution curve C_ν can play the role of a boundary data at $r = R$. Because of the scale invariance (11), a given point (u_R, v_R) represents a one parameter family of boundary data, $\{(e^s M_R, e^s R, e^{-2s} T), s \in \mathbb{R}\}$, characterized by the scaling s . Rather than using the boundary data, we characterize a solution by identifying (ν, r_H, R) .

A. Regular solutions

Before dealing general solutions, let us illustrate a well-known solutions in Refs. [2–4]. Most results in this subsection are reproductions of theirs except a few details. The purpose of this subsection is to illustrate the role of a solution curve C in (u, v) plane obtained by numerically integrating Eq. (7) or (4). The curve C is given in Fig. 1 (a). An important property of the solution curve is its uniqueness. The value ν_r presented just after Eq. (23) is given by obtaining $u_H \approx 0.4926$ for the solution curve. A typical mass and density profiles for a specific solution are shown in Fig. 1 (b).

The solution curve C begins with $u = 0 = v$ at $r = 0$. On the curve v takes its maximal value $v_P \approx 0.3416$ at P and u takes its maximum $u_H \approx 0.4926$ at H . The ratio of the radial coordinates between P and H is $r_P/r_H \equiv e^{\xi_P} \approx 0.4823$. The allowed range of u and v are restricted to $0 \leq u \leq u_H$ and $0 \leq v \leq v_P$, respectively. Eventually, the curve spirals in to the point $\mathcal{R}(3/7, 3/14)$. From the analysis of the heat capacity in Ref. [3], a thermodynamic instability is set on for a system having the outer boundary in the region from P to H . Interestingly, the heat capacity for a system having the outer boundary just outside the point H is positive definite.

The density at the center is $\rho(0) = \kappa(8\pi r_H^2)^{-1}$, where $\kappa \approx 4.759$, and monotonically decreases with r . The central form of mass is given by $m_r(r)$ in Eq. (13). For $r \gg r_H$, the mass increases linearly.

B. Solutions with a conical singularity at the center

For $0 < \nu < \nu_r$, the solutions have a conical singularity at the center. In Fig. 2, we plot solution curves for various values of ν in this range. For comparison, the solution curves for the regular solution is denoted as the red curve. An interesting difference from the regular-solution curve is apparent. The curves begin at $(u, v) \rightarrow (-\infty, 0)$ at $r = 0$, where the negative value of u is due to the negative mass of conical singularity. Because of this, the range of the picture is extended to include negative u . For $\nu \sim \nu_r$, the solution curve stays close to the line $v = 0$ for $u < 0$. Then, the curve converges to that of the regular solution for $u > 0$. For a smaller ν , the solution curve departs $v \approx 0$ earlier. On the whole, the curve $C_{\nu(<\nu_r)}$ lies outside of the regular solution curve C . In the asymptotic regime, the curves spiral in to the point \mathcal{R} similarly to C .

The maximum value of u for a given solution curve C_ν is given by

$$u_H = 1 - \nu, \quad v_H = \frac{1 - \nu}{2}. \quad (25)$$

The maximum value of $v = v_{P_\nu}$ for a given solution curve C_ν monotonically increases as ν decreases from ν_r . For a given ν , the value r_P/r_H decreases with ν as in Fig. 3. Those functions are roughly approximated by

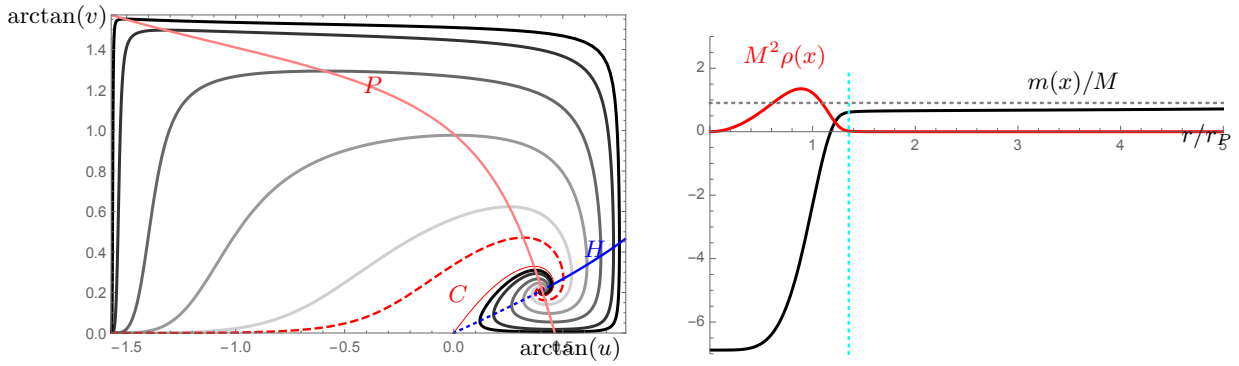


FIG. 2: The solution curves (Left), mass and density distribution (Right). In the left figure, each curve corresponds to $\nu = \nu_r, 0.45, 0.4, 0.3, 0.2, 0.1$, and 0.05 , respectively from the bottom. The blue curve H represents the referential position. The thick pink curve P denotes the position where v is maximized on solution curves. In the right figure, the typical behavior of mass and density is given. This figure corresponds to $\nu = .1$. The dotted cyan line denotes where a *fake horizon* forms.

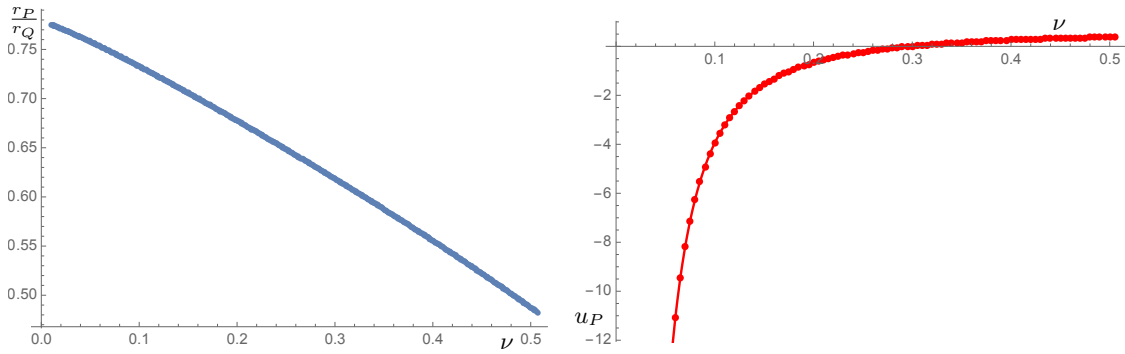


FIG. 3: The values of r_P/r_Q and u_P with respect ν .

$$\frac{r_P}{r_H} = 0.7807 - 0.4519\nu - 0.3383\nu^2 + \dots, \quad (26)$$

Note that the ratio is a function of ν only and monotonically decreases with ν . At $\nu = \nu_r$, the ratio becomes $r_P/r_H \approx 0.4823$, which value is the same as that of the regular solution. The value of u_P is approximated by

$$u_P \approx -0.03558\nu^{-2} - 0.1271\nu^{-1} + 0.9246 - 0.3858\nu + \dots.$$

For $\nu \ll 1$, it goes to negative infinite quadratically.

An interesting merit of parametrization of the central region in Eqs. (14) and (15) is that the values of μ_0 and κ are functions of ν only. In Fig. 4, we plot how the values at the central region change with respect to ν . Both monotonically decreases with ν and they diverge as $\nu \rightarrow 0$. Numerically, the values are well approximated by,

$$\begin{aligned} \mu_0 &\approx 0.0771\nu^{-2} + 0.2136\nu^{-1} - 1.2077 + 1.0067\nu + \dots, \\ \kappa &\approx 1.049\nu^{-2} + 5.872\nu^{-1} + 12.93 + 71.90\nu - 114.7\nu^2 + \dots, \end{aligned} \quad (27)$$

where the range is $0 < \nu < \nu_r$. A discrepancy of this numerical result is that the plots in Fig. 4 fails to reproduce the regular solution result for $\nu = \nu_r$ where $\mu_0 = 0$ and $\kappa \approx 4.759$. This is because the equations in Eq. (27) are expanded around $\nu = 0$.

IV. ANALYTIC TREATMENT OF A SELF-GRAVITATING RADIATION IN A SPHERICAL SHELL AROUND A STRONG FAKE HORIZON

A strong *fake horizon*, which is a *fake horizon* with $\nu \sim 0$, is an especially interesting object because it is on the verge of becoming a true event horizon in the sense that $m(r_{\text{th}}) \approx r_{\text{th}}/2$. We hope that this interesting case allows an

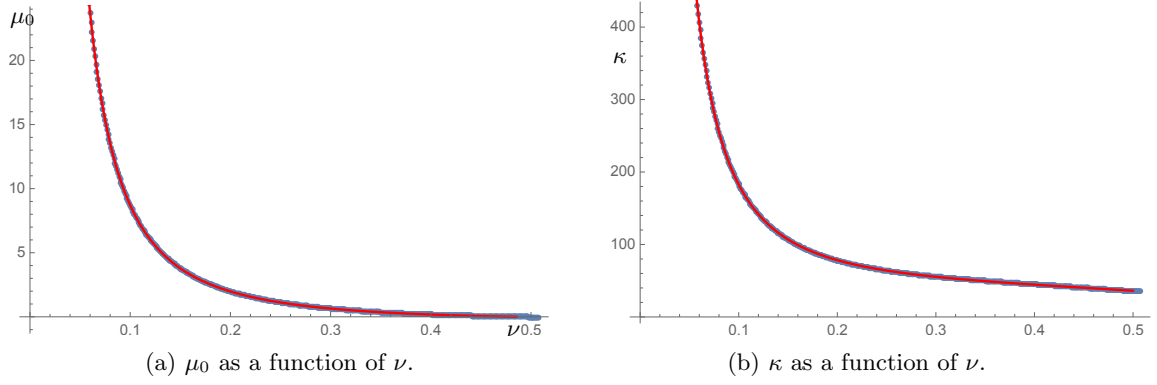


FIG. 4: The change of μ_0 and κ as a function of ν . The approximate functional form are given as red curves.

analytic description, which turns out to be true. Part of the present results were given in Ref. [23] where the authors assumed the temperature to be the Hawking temperature. At the present work, we do not take the assumption because it is not always proper. The *fake horizon* is different from a blackhole horizon even though it has some similarity. A solution curve C_ν in the presence of a strong *fake horizon* is given in Fig. 5. For simplicity, we represent

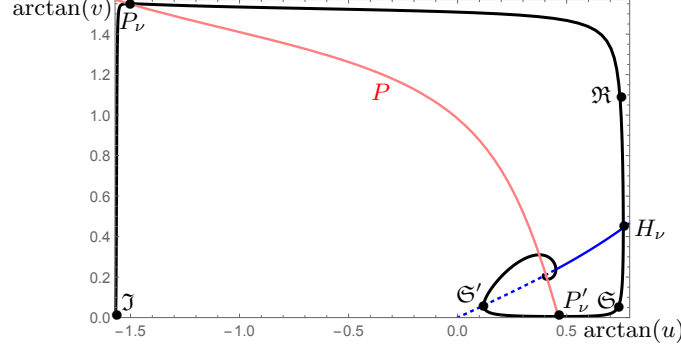


FIG. 5: Solution curve (black) for systems having strong *fake horizon*. The point \mathcal{J} represents $(u, v) = (-\infty, 0)$.

a segment of the solution curve by using its boundary points. For example, $[P_\nu, \mathfrak{R}]$ represents the segment from the point P_ν to the point \mathfrak{R} . A *fake horizon* is in the segment $[\mathfrak{R}, \mathfrak{S}]$. There, u is almost constant but v changes a lot. The segment $[\mathfrak{S}, \mathfrak{S}']$ is located just outside of the *fake horizon*. v remains close to zero and u decreases monotonically with r . For $\nu \approx 0$, most of the mass is located inside the *fake horizon*.

Let us first analyze the segment $[\mathfrak{R}, \mathfrak{S}]$ of the solution curve depicted in Fig. 5, which denotes the near *fake horizon* region. On the segment, u changes slowly with $u \approx u_H \approx 1$ if $\nu = 1 - u_H \ll 1$, which plays the role of a parameter measuring how close the *fake horizon* is to the event horizon. Solving Eq. (7) keeping first non-vanishing corrections of $O(\nu)$, one get

$$1 - u \approx \varepsilon \frac{(2v/3 + 1)^2}{\sqrt{2v}} + O(\varepsilon^2), \quad \frac{1}{2}\varepsilon^2 \ll v_{\mathfrak{S}} < v < v_{\mathfrak{R}} \ll \frac{1}{2}\left(\frac{9}{\varepsilon}\right)^{2/3}, \quad (28)$$

where $\varepsilon = 9\nu/16$ is the expansion parameter. We choose the points \mathfrak{R} and \mathfrak{S} so that $v_{\mathfrak{R}} = \varepsilon^{-1/3}$ and $v_{\mathfrak{S}} = \varepsilon^{2/3}/2$. Integrating Eq. (6) and using Eq. (5), we get

$$r = r_H e^\xi; \quad \xi = \frac{\varepsilon}{\sqrt{2v}} \left(1 - \frac{v}{6}\right) - \frac{11\varepsilon}{12}, \quad (29)$$

where we choose $\xi = 0$ at H . Note that r changes only a bit for a large change of v in $[\mathfrak{R}, \mathfrak{S}]$. The mass inside and the density at r are, keeping dominant contribution only, given by

$$m(r(v)) = \frac{r_H}{2} e^{\xi} u \approx \frac{r_H}{2} \left[1 - \frac{\varepsilon(2v)^{3/2}}{9} \left(1 + \frac{27}{8v}\right) - \frac{11\varepsilon}{12} \right]. \quad (30)$$

The relative increase of the mass from \mathfrak{R} to \mathfrak{S} is $(m_{\mathfrak{S}} - m_{\mathfrak{R}})/m_{\mathfrak{R}} \approx 2^{3/2}/9 \times \varepsilon^{1/2}$, which is relatively small compared to $m_{\mathfrak{R}}$. On the other hand, the density, $\rho = v/4\pi r^2$, decreases rapidly in $[\mathfrak{R}, \mathfrak{S}]$ so that $\rho(r_{\mathfrak{S}})/\rho(r_{\mathfrak{R}}) \approx \varepsilon/2$, because ρ is roughly proportional to v . This implies that the density profile in r is extremely steep.

We next analyze the segment $[\mathfrak{S}, \mathfrak{S}']$ of the solution curve depicted in Fig. 5, where $u_{\mathfrak{S}} \approx 1$ and $0 < u_{\mathfrak{S}'} \ll 1$. In the region of interest, $v \ll 1$ and $dv < du$. The solution curve C_{ν} , solving Eq. (7) up to first nonvanishing order, is described by

$$v = \frac{\varepsilon^2}{2u^2(1-u)^2}; \quad \varepsilon^{2/3} \ll u_{\mathfrak{S}'} \equiv \varepsilon^{\beta} < u < u_{\mathfrak{S}} = 1 - \varepsilon^{2/3}. \quad (31)$$

We identify the two curves in Eqs. (28) and (31) at \mathfrak{S} , satisfying $du = dv$. The radius can be obtained by integrating Eq. (6) using Eq. (31). To the first nonvanishing correction, we get

$$r = r_H e^{\xi} \approx \frac{r_H}{u} \exp \left[-\frac{11\varepsilon}{12} + \frac{\varepsilon^2}{3u^3} \right] \Rightarrow u \approx \frac{r_H}{r} \left[1 - \frac{11\varepsilon}{12} + \frac{\varepsilon^2}{3} \left(\frac{r}{r_H} \right)^3 \right], \quad (32)$$

where we keep terms to $O(\varepsilon^1)$ and we choose $\beta = 1/3$. Now, the range of the radius for the segment is given by $r_H < r < \varepsilon^{-1/3} r_H$. The radius increases almost inverse linearly with u . The segment $[\mathfrak{S}, \mathfrak{S}']$ corresponds to the long quasi-asymptotic region given by $u_t(\xi)$ in Eq. (19). Note that the mass $m(r) = r_H/2$ is included in the surface $r = (11/4\varepsilon)^{1/3} r_H$.

Outside the surface \mathfrak{S}' , near $0 < u, v \ll 1$, the solution curve approaches that of the regular solution. The function u takes exactly the same form as that in Eq. (32). On the other hand $v = (\varepsilon^2/2) \times (r/r_H)^2$. Therefore, from the point of view of a far outside observer, the geometry appears to be a combination of a blackhole of mass, $m_{\text{bh}} = r_H(1 - 11\varepsilon/12)/2$, surrounded by a constant density, $\rho_0 = \varepsilon^2/(8\pi r_H^2)$.

Finally, we consider the segment $[\mathfrak{J}, \mathfrak{R}]$ which corresponds to the region far inside the *fake horizon*. In the region $u \ll 1$ and $2v - u \gg 1$ are satisfied. As was done in Ref. [23], Eq. (7) and (6) can be approximately solved to give

$$v \equiv \frac{15/2}{(r_H/r)^5 - 1} (1 - u) = \frac{1}{2} \left(\frac{3}{5\varepsilon} \right)^2 \left(\frac{r}{r_H} \right)^4 \left[1 - \left(\frac{r}{r_H} \right)^5 \right]^2. \quad (33)$$

v takes its maximum value $v_{\text{max}} = (7/2)^{1/5} 9/7^3 \varepsilon^2$ at $r = r_{\text{max}} \equiv (2/7)^{1/5} r_H$, where the integration constant is determined by matching the value of $1 - u$ at \mathfrak{R} with Eqs. (28) and (29). The value of u at the maximum point is $u_{\text{max}} = 1 - v_{\text{max}}/3$. From Eq. (7), the point that maximize v must be located on the line P given in Eq. (8), which is not satisfied by $(u_{\text{max}}, v_{\text{max}})$. This indicates that Eq. (33) is an approximate solution with error of $O(1/v_{\text{max}})$, which becomes negligible if the limit $v_{\text{max}} \gg 1$ is taken into account. Note also that $r_{\text{max}}/r_H = (2/7)^{1/5} \approx 0.7783$ is close to the numerically fitting value in Eq. (26).

Finally, comparing the $r \rightarrow 0$ limit of Eq. (33) with Eqs. (15) then using Eqs. (3) and (6), we get the limiting forms for $\nu \ll 1$ as

$$\mu_0 = \frac{2}{15} \left(\frac{16}{15} \right)^2 \nu^{-2}, \quad \kappa = \left(\frac{16}{15} \right)^2 \nu^{-2}. \quad (34)$$

This implies that both μ_0 and κ diverge quadratically as $\nu \rightarrow 0$. Both coefficients are close to their numerical fitting values in Eq. (27). Note that the resulting form for the bare mass $m(0) \equiv -r_H \mu_0/2 \propto -r_H/\nu^2$ is formally different from that in Ref. [23] ($\propto -r_H^3$). The difference comes from the fact that the temperature was treated to be that of the blackhole there.

V. SUMMARY AND DISCUSSIONS

We studied a system of self-gravitating radiation confined in a spherical box by using numerical and analytic calculations. We classified the solution space systematically and defined a *fake horizon* from the similarity with apparent horizon. We found an analytic solution describing a system having a *fake horizon* whose limiting geometry resembles an apparent horizon.

Assuming the box to be large enough so that its boundary is located in the asymptotic region, the behavior of the solutions can be summarized as follows: The geometry outside the box is described by the Schwarzschild metric. Around the center, the mass behaves as $m_r \propto r^3$ or $m_s \propto -m_0 + r^5$ in the absence or in the presence of a central conical singularity, respectively, where r is the areal radial coordinate. On the other hand, for large r , the asymptotic form follows a single formula $m_a \propto 3r/14$. In between the two limits, a *fake horizon* appears. If the *fake horizon* is

close to an apparent horizon, the transient state $m_t \sim r_{\text{fh}}/2 + \epsilon^2 r^3$ arises for a wide range of r just outside of the *fake horizon*, where ϵ is a very small number.

To classify the solutions, we have designed a set of parameters which characterize both the internal geometry and the macroscopic quantities. The first parameter ν identifies a solution curve C_ν , a curve on the two dimensional space of scale invariant variables $(u, v) \equiv (2m(r)/r, 4\pi r^2 \rho(r))$, which satisfy a first order differential equation originated from the Tolman-Oppenheimer-Volkoff equation. Here, ν represents the minimum value of $1 - u$ for a given solution curve, where the minimum is accomplished on the *fake horizon*. In this sense, ν measures how much a *fake horizon* differ from an apparent horizon. The value of ν is limited to a finite domain $0 \leq \nu \leq \nu_r \approx 0.50735$. For $\nu = 0$, the *fake horizon* becomes an apparent (event) horizon. Only for $\nu = \nu_r$, the solution is absent of singularity. Any solution other than the regular one has a conical singularity at the origin. The second parameter r_H represents the size of the *fake horizon*. It determines the scale of the specific solution curve C_ν . Any point on C_ν is parameterized by $(u(\xi), v(\xi))$ where $\xi = \log(r/r_H)$ where $u(\xi)$ and $v(\xi)$ are parameterized functions of ξ determining C_ν . The last parameter is the star size R . Given the three parameters (ν, r_H, R) , the ADM mass and the surface temperature are given by $M_R = Ru(\xi_R)/2$ and $T = (v(\xi_R)/4\pi\sigma R^2)^{1/4}$, respectively, where $\xi_R = \log(R/r_H)$. Many important physical properties are determined by the position of the boundary on the solution curve. For example, if $R > r_H$, the box includes the *fake horizon*. If $R < r_H$, the density at the surface will be very high and the contribution of the radiation to the mass is maximized near the surface. For the case of a regular solution, the sign of the heat capacity for a self-gravitating system [3] is also determined by the position on the solution curve.

With respect to the behavior near the central singularity, we found a mass formulae approximately with respect to the variation of ν . In the $\nu \rightarrow 0$ limit, the coefficients for the mass function behave as $1/\nu^2$ which were shown to be correct in the limit by using analytic calculation. The mass formula will be useful when one study the behavior of the central conical singularity with respect to the change of macroscopic quantities. In studying the stability of the system, the heat capacity plays a central role. However, the calculation of the heat capacity is nontrivial because of the central singularity of which thermodynamic properties we do not know. If it is possible to ignore the singularity, the heat capacity is determined by the same way as that of the regular solution in Ref. [3]. In that case, the heat capacity for systems having boundary just inside of the *fake horizon* is negative definite. On the other hand, the heat capacity just outside is positive definite even with the geometrical similarity to the event horizon. Far outside of it, a wide approximately constant mass region appears. The geometry in this region resembles that of the Schwarzschild blackhole with a radiation field. Systems having boundary in this region have negative heat capacity once more. Whereas, there is a proposal for the thermodynamic properties of the central singularity [22]. Because of this complexity, the stability [5, 6] issues should be dealt cautiously.

Acknowledgment

This work was supported by the National Research Foundation of Korea grants funded by the Korea government NRF-2013R1A1A2006548.

-
- [1] D. Lynden-Bell and R. Wood, Mon. Not. R. Astr. Soc. **138**, 495 (1968).
 - [2] R. D. Sorkin, R. M. Wald and Z. J. Zhang, Gen. Rel. Grav. **13**, 1127 (1981).
 - [3] D. Pavon and P. T. Landsberg, Gen. Rel. Grav. **20**, 457 (1988).
 - [4] P. H. Chavanis, Astron. Astrophys. **483**, 673 (2008) [arXiv:0707.2292 [astro-ph]].
 - [5] P. H. Chavanis, Astron. Astrophys. **381**, 340 (2002) doi:10.1051/0004-6361:20011438 [astro-ph/0103159].
 - [6] P. H. Chavanis, C. Rosier and C. Sire, Phys. Rev. E **66**, 036105 (2002) doi:10.1103/PhysRevE.66.036105 [cond-mat/0107345].
 - [7] H. J. Schmidt and F. Homann, Gen. Rel. Grav. **32**, 919 (2000) [gr-qc/9903044].
 - [8] M. Schiffer and J. D. Bekenstein, Phys. Rev. D **39**, 1109 (1989). doi:10.1103/PhysRevD.39.1109
 - [9] S. Hod, gr-qc/9901035.
 - [10] S. Gao, Springer Proc. Phys. **170**, 359 (2016). doi:10.1007/978-3-319-20046-043
 - [11] S. Gao, Phys. Rev. D **84**, 104023 (2011) [Phys. Rev. D **85**, 027503 (2012)] doi:10.1103/PhysRevD.84.104023, 10.1103/PhysRevD.85.027503 [arXiv:1109.2804 [gr-qc]].
 - [12] X. Fang and S. Gao, Phys. Rev. D **90**, no. 4, 044013 (2014) doi:10.1103/PhysRevD.90.044013 [arXiv:1311.6899 [gr-qc]].
 - [13] J. P. S. Lemos, arXiv:0712.3945 [gr-qc].
 - [14] C. Anastopoulos and N. Savvidou, Class. Quant. Grav. **31**, 055003 (2014) doi:10.1088/0264-9381/31/5/055003 [arXiv:1302.4407 [gr-qc]].
 - [15] R. Bousso, Rev. Mod. Phys. **74**, 825 (2002) doi:10.1103/RevModPhys.74.825 [hep-th/0203101].
 - [16] R. D. Sorkin, gr-qc/9705006.

- [17] D. N. Page, JCAP **1406**, 051 (2014) doi:10.1088/1475-7516/2014/06/051 [arXiv:1306.0562 [hep-th]].
- [18] D. N. Page and K. C. Phillips, Gen. Rel. Grav. **17**, 1029 (1985). doi:10.1007/BF00774206
- [19] V. Vaganov, arXiv:0707.0864 [gr-qc].
- [20] S. A. Gentle, M. Rangamani and B. Withers, JHEP **1205**, 106 (2012) doi:10.1007/JHEP05(2012)106 [arXiv:1112.3979 [hep-th]].
- [21] A. Pesci, Class. Quant. Grav. **24**, 2283 (2007) doi:10.1088/0264-9381/24/9/009 [gr-qc/0611103].
- [22] C. Anastopoulos and N. Savvidou, Class. Quant. Grav. **29**, 025004 (2012) [arXiv:1103.3898 [gr-qc]].
- [23] W. H. Zurek and D. N. Page, Phys. Rev. D **29**, 628 (1984).